

**Quantum calculations of the rate constant for the  $O(^3P) + HCl$   
reaction on new *ab initio*  $^3A''$  and  $^3A'$  surfaces**

Tiao Xie,<sup>a</sup> Joel M. Bowman,<sup>a,\*</sup> K. A. Peterson,<sup>b</sup> and B. Ramachandran<sup>c</sup>

<sup>a</sup> Department of Chemistry and Cherry L. Emerson Center for Scientific Computation,  
Emory University, Atlanta, GA 30322

<sup>b</sup> Department of Chemistry, Washington State University, Pullman, WA, 99164-4630

<sup>c</sup> Chemistry, College of Engineering & Science, Louisiana Tech University, Ruston, LA  
71272

Submitted to J. Chem. Phys.

---

\* email address: [bowman@euch4e.chem.emory.edu](mailto:bowman@euch4e.chem.emory.edu)

## ABSTRACT

We report the thermal rate constant of the  $O(^3P) + HCl \rightarrow OH + Cl$  reaction calculated from 200 to 3200 K, using new fits to extensive *ab initio* calculations [B. Ramachandran and K. A. Peterson, *J. Chem. Phys.* preceding paper]. The rate constants are obtained for both the  $^3A''$  and  $^3A'$  surfaces using exact quantum reactive scattering calculations for selected values of the total angular momentum and the *J*-shifting approximation for both the  $^3A''$  and  $^3A'$  surfaces. The results are compared with the ICVT/ $\square$ OMT rate constants calculated by the POLYRATE program and all available experimental data. Other related high energy reaction channels are also studied qualitatively for their contribution to the total thermal rate constant at high temperature.

## I. INTRODUCTION

The  $O(^3P) + HCl \rightarrow OH + Cl$  reaction has become one of the most extensively studied chemical reactions. The first quantum calculations of the thermal rate constants on an *ab initio* potential energy surface were reported by Koizumi, Schatz, and Gordon (KSG),<sup>1</sup> who developed a global potential based on MP2/6-31G(d) calculations. These workers investigated some complexities in this reaction, owing to the open shell O atom and the ‘heavy-light-heavy’ kinematics of the reaction. In particular they noted that the reaction has two possible reaction paths through the  $^3A''$  and  $^3A'$  electronic states. They found that the lower energy reaction path passes through the bent  $^3A''$  transition state. The KSG potential for the  $^3A''$  electronic state has been used in numerous quantum calculations of the rate constant.<sup>1-8</sup>

These calculations revealed resonances in the cumulative reaction probability (CRP) due to the “heavy-light-heavy” mass combination of this reaction. They appeared at fairly high energies and thus did not have significant impact on the thermal rate constant, except possibly at very high temperatures. The rate constants calculated using accurate quantum methods on the KSG potential surface are too high by factors of 2 to 3 for temperatures below 500 K compared to experimental data. This led to the speculation that the reaction barrier on the KSG potential surface was too low.

Subsequently a newer  $^3A''$  potential surface, with an adiabatic barrier 1.35 kcal/mol higher than the KSG one, was reported by Ramachandran *et al.*<sup>9</sup> (the surface is referred to as “S4”). This potential was used in variational transition state theory (VTST) calculations with a sophisticated semiclassical treatment of tunneling on the rate constant (denoted ICVT/ $\square$ OMT)<sup>10</sup> using the code ‘POLYRATE’.<sup>11</sup> Very good agreement

with experiment was obtained throughout a large temperature range, including the significant range below 500 K. However, when this potential was used in quantum calculations (which were exact for zero total angular momentum,  $J$ , and used  $J$ -shifting<sup>12</sup> for non-zero  $J$ ) of the rate constant,<sup>7,8</sup> the results exceeded experiment for temperatures below 500 K, and were fortuitously in quite good agreement with rate constants using the KSG potential despite the higher barrier on the S4 surface. (Thus, these quantum calculations are in disagreement with ICVT/ $\square$ OMT rate constants as well, at temperatures below 500 K.<sup>10</sup>) The source of this somewhat surprising result was traced to the existence of van der Waals wells on the S4 surface in the entrance and exit channels. At low energy, i.e., below the vibrationally adiabatic barrier height, resonances were found in the CRP for the S4 surface. A detailed analysis of these resonances<sup>13</sup> showed that they are due to these van der Waals wells. The increase of the rate constant relative to expectation and also relative to the 'POLYRATE' results (which are not sensitive to these wells) was therefore ascribed to these van der Waals wells.

As a result of this somewhat surprising result a major effort was undertaken by Ramachandran and Peterson (RP) to obtain highly accurate and hopefully definitive potentials for this reaction. The details and results of this effort are reported in the preceding paper.<sup>14</sup> The highlights of the RP surfaces are: the ground-state vibrationally adiabatic barrier height is 8.83 kcal/mol for the  $^3A''$  surface (this is higher by 0.70 kcal/mol than the corresponding barrier on the S4 surface) and the analogous barrier on the new potential for the  $^3A'$  state is 11.97 kcal/mol. This higher barrier suggests that the  $^3A'$  surface would only be expected to contribute significantly at high temperatures.

Here we report quantum calculations of the thermal rate constants using these new potentials and compare the results with experiments, including new measurements at high temperature.<sup>15,16</sup> The new RP  $^3A''$  surface does contain van der Waals wells in both the entrance and exit channels and, similar to the S4 surface, these do lead to low energy resonances in the CRP in quantum scattering calculations. However, these low energy resonances and their relation to the van der Waals wells, which have been previously explored extensively in the case of the S4 surface,<sup>13</sup> are not the focus of this paper.

Details of the calculations are given in the next section. Extensive testing of the  $J$ -shifting approximation is also given in that section because the present calculations must extend to high values of  $J$  and high energies in order to obtain the rate constant up to 3200 K. The results of the calculations, comparisons with experiment and ICVT/ $\square$ OMT calculations, and discussion of these comparisons are given in Section III. A summary and conclusions are given in Section IV.

## II. METHODS AND DETAILS OF THE CALCULATIONS

### A. Quantum calculations

The exact thermal rate constant can be written as

$$k(T) = \frac{1}{hQ_{react}(T)} \int_0^\infty N(E) e^{-E/k_B T} dE,$$

where  $E$  is the total energy,  $Q_{react}$  is reactant partition function (the product of the translational partition function and the internal vibration-rotation-electronic partition function), and  $N(E)$  is the cumulative reaction probability (CRP). The exact CRP is defined as the sum of all allowed state-to-state reaction probabilities, which for the present atom-diatom reaction, is given by

$$N(E) = \sum_{J=0}^{\infty} (2J+1) \sum_{v'j'K'} P_{vjK,v'j'K'}^J(E), \quad (1)$$

where  $P_{vjK,v'j'K'}^J(E)$  is the detailed state-to-state reaction probability for a given total angular momentum  $J$  and  $K$  ( $K'$ ) is the projection quantum number of  $J$  on a body-fixed Z-axis. It is very computationally intensive to calculate these probabilities over the large range of  $J$  that is needed to obtain the rate constant over a large temperature range. A very useful approximation to  $N(E)$  is the  $J$ -shifting approximation, given by<sup>12</sup>

$$N(E) = \sum_{J=0}^{\infty} (2J+1) \sum_{K=0}^J N^{J=0}(E - E_{J,K}^\ddagger), \quad (2)$$

where  $E_{J,K}^\ddagger$  is the rotational energy of the transition state, and  $N^{J=0}$  is the CRP for  $J=0$  (in which case  $K=0$ ). The OHCl  $^3A''$  transition state is a near prolate top, with rotation constants  $A^\ddagger > B^\ddagger \approx C^\ddagger$ , and so  $E_{J,K}^\ddagger$  is given by  $\bar{B}^\ddagger J(J+1) + [A^\ddagger - \bar{B}^\ddagger] K^2$ , where ( $\bar{B}^\ddagger$  is

the average of  $B^\ddagger$  and  $C^\ddagger$ ). This approximation has been tested extensively for the rate constant of the  $O(^3P)+HCl$  reaction on both the KSG<sup>2-4</sup> and S4<sup>7,8</sup> potentials and was found to be accurate to within 30% or less for temperatures between 200 and 1000 K. Because we wish to extend the temperature range to 3000 K, additional tests of this approximation are made here.

As mentioned above, the  $^3A'$  surface may also play a role in this reaction at high temperatures, and thus we also calculate the rate constant for this potential. Unlike the  $^3A''$  surface, the  $^3A'$  surface has a collinear transition state. This is obviously a special case for  $J$ -shifting, since no  $A$ -constant is defined. In this case  $K$  takes the role of the vibrational angular momentum quantum number,<sup>12</sup> and is thus one of two quantum numbers that describe the doubly-degenerate bending motion of the transition state. In reactions such as the present one, where the bending frequency is several hundreds of wavenumbers, the range of  $K$  needed to converge the CRP is generally much less than  $-J$  to  $+J$ . There are versions of  $J$ -shifting that can be applied in this case, as described elsewhere.<sup>12</sup> Here we do the more elaborate treatment of the  $J$ -shifting, where exact scattering calculations are done for a limited range of  $J$  and thus with a maximum value of  $K$ , denoted  $K_{max}$ , and then  $J$ -shifting is done for larger  $J$  using  $E_{J,K}^\ddagger = \bar{B}^\ddagger J(J+1)$  for the rotational energy.

The quantum scattering calculations were done with the code 'ABC'.<sup>17</sup> In these calculations, we retain all reactant and product channels with internal energies less than  $E_{max} = 3.5$  eV [relative to  $O + HCl(r_e)$ ] and with diatomic rotational quantum numbers less than or equal to  $j_{max} = 25$  for the  $^3A''$  surface or  $j_{max} = 20$  for the  $^3A'$  surface. The close-coupled equations were integrated using 125 hyperradii sectors between  $\varphi_{min} =$

2.2 bohr for the  ${}^3A''$  surface or 2.3 bohr for the  ${}^3A'$  surface and  $\Delta_{max} = 16.0$  bohr. The value of  $K_{max}$  varied depending on the potential surface. This will be discussed in more detail in the next section.

Finally, as usual, to account for the spin-orbit splitting of the oxygen atom and saddle point electronic states, the rate constants have been multiplied by a factor to represent the fraction of collisions that correlate with the reactive  ${}^3A''$  or  ${}^3A'$  surface, which is given by<sup>1,7</sup>

$$f(T) = 3 / (5 + 3e^{-\Delta_{228}/T} + e^{-\Delta_{326}/T}).$$

At high temperature,  $f(T)$  is roughly 1/3, which represents the ratio of the degeneracy of the  ${}^3A''$  or  ${}^3A'$  surface (3) and  ${}^3P$  oxygen atom (9) without spin-orbit splitting.

## B. Variational transition state theory calculations

The VTST calculations are similar to those reported earlier for the S4 surface.<sup>10</sup> The thermal rate constant calculations for the present paper were carried out with the POLYRATE program<sup>11</sup> using curvilinear internal coordinates,<sup>18</sup> and the harmonic approximation for the vibrational modes. The  ${}^3A''$  surface has a stretch and a nondegenerate bend mode orthogonal to the reaction path while the  ${}^3A'$  surface, with its collinear minimum energy saddle point, has a stretch and a degenerate bend mode to be represented in this fashion. In the case of the  ${}^3A''$  surface, a non-collinear reference path was used. The range of the reaction path was chosen to be large enough that both the entrance and exit channel vdW wells were sampled. The improved canonical variational theory (ICVT)<sup>19,20</sup> was used to calculate the thermal rate constants and semiclassical estimates of quantum mechanical tunneling were obtained using the

microcanonical optimized multidimensional tunneling ( $\mu$ OMT) approximation.<sup>21</sup> The resulting ICVT/ $\mu$ OMT rate constants are reported in the following Section.

### III. RESULTS AND DISCUSSION

#### A. Quantum reactive scattering calculations and tests of $J$ -shifting

In Fig. 1 the exact quantum  $J = 0$  CRPs for the  $^3A''$  and  $^3A'$  surfaces are plotted against the total energy up to 2.75 eV. As seen, there is distinct resonance structure in the  $^3A''$  CRP in the energy region below the vibrationally adiabatic barrier (which has a total energy of 0.57 eV with respect to the Born-Oppenheimer entrance channel minimum), while the  $^3A'$  curve is very smooth. These resonances are due to the van der Waals wells on the  $^3A''$  potential energy surface. As noted in the preceding paper, such wells are not present on the  $^3A'$  surface, and so this specific difference in the CRPs is expected. Another difference is that the  $^3A'$  CRP is shifted up in energy relative to the  $^3A''$  one. Much of this positive shift is due to the higher barrier on the  $^3A'$  surface. However, some of the shift is also due to the fact that the saddle point of the  $^3A'$  surface has a collinear geometry and thus the  $J = 0$  CRP contains contributions only from the even bend states of the transition state (because  $K = 0$ ).<sup>12</sup> The odd bending states occur for  $J \geq 1$ . For the even parity component of the  $J = 1$  CRP only the odd bending states contribute for the  $^3A'$  CRP. This CRP is shown in Fig. 2 along with the  $J = 0$  CRP, which as noted already has contributions only from the even bending states. At low energies the even parity component of the  $J = 1$  CRP is shifted by 0.046 eV from the  $J = 0$  CRP, which is approximately equal to the harmonic bending energy of the  $^3A'$  linear

transition state.

It is possible to approximately account for this bending energy shift of the  $J = 1$  CRP relative to the  $J = 0$  by using a suitable modification of  $J$ -shifting.<sup>12</sup> We take a somewhat different approach here. First we determined the maximum value of  $K$  needed to obtain a converged CRP for a moderately large value of  $J$ . This was done by performing a series of calculations for  $J = 50$  with  $K_{max} = 4, 6, 8, 10$ , and the maximum possible value of  $K$ . The results are shown in Fig. 3 (for odd parity) versus the total energy. As seen, the CRP with  $K_{max} = 10$  is well converged over this energy range. That the converged value of  $K_{max}$  would be relatively small is a consequence of the “tight” collinear transition state where, as noted earlier,  $K$  takes the role of the vibrational angular momentum. In the harmonic approximation  $K = 10$  first occurs for the ninth excited bending state, the energy of which would raise the adiabatic energy by roughly 0.5 eV. Then, to obtain the full CRP for the  ${}^3A'$  surface, exact calculations were done for  $J \leq 10$  (with  $K_{max} \leq 10$ ) and then  $J$ -shifting was done for  $J > 10$  using the equation

$$N^J(E) = N^{J=10} \{E \square B^\ddagger [J(J+1) \square 110]\}, \quad (3)$$

where the  ${}^3A'$  collinear saddle point  $B^\ddagger$ -constant is used in this equation. A test of the approximation is shown in Fig. 4, where the energy dependence of the CRP for  $J = 50$ , with  $K_{max} = 10$ , is compared to the one using eq. (3). As seen, the approximation is accurate to within a few percent over the full energy range. This approximation [eq. (3)] was used to obtain the CRP up to total energies of 2.76 eV, where  $J$  values as large as 300 are necessary to obtain a converged result.

For the calculation of the thermal rate constant on the  ${}^3A'$  surface the “standard”  $J$ - $K$

shifting approach, eq. (2), can be applied. However, as noted already, since we are interested in obtaining the rate constant to temperatures as high as 3200 K, we need to test the accuracy of this approach for high total energy and large values of  $J$ . To test the accuracy of the  $J$ -shifting approximation under these extreme conditions, we calculated benchmark CRPs for some large  $J$  values and compared them with the ones from the  $J$ -shifting approximation. Four sets of scattering calculations were run with  $J = 20, 70, 130,$  and  $200$  at three total energies each. For each calculation, a restriction of  $K_{max} = 15$  was applied to reduce the computational effort. This value of  $K_{max}$  was tested by comparison against an exact  $J = 20$  (odd parity) CRP and was shown to be accurate to within 5% or less over the full energy range. (This exact calculation for  $J = 20$  resulted in a coupled channel basis of 5708 and took roughly 9 days on a Compaq Alpha ES45 workstation, 1.8 GHz processor.) These benchmark CRPs are plotted in Fig. 5(a) along with the corresponding ones from the  $J$ -shifting approach using eq. (2). It is clear that there are some significant errors in the approximation for high values of  $J$  and at the highest energies. The highest total energy considered in this plot, 2.75eV, is more than 4 times higher than that of the ground-state vibrationally adiabatic barrier (0.57eV). At such a high energy, one might expect that  $J$ -shifting with the transition state rotational constants might start to fail. A simple “fix” to this problem is to use a different set of rotational constants. (This has been shown to work quite well for the H+H<sub>2</sub> reaction,<sup>22</sup> where there is just a B-constant to consider.) The simple approach we took was to fix the  $A$ -constant at the saddle point value and determine an empirical  $B$ -constant to obtain improved agreement between  $J$ -shifting and exact results for the four  $J$  values at the 3 energies given in Fig. 5(a). Of course a single value is not obtained; however, all

the results were quite close to the rough average value of  $B_{opt} = 2.35 \times 10^{-5}$  eV, which is 23% smaller than the saddle point  $B$ -constant. The CRP's calculated with this optimal value are compared to the benchmark CRP's in Fig. 5(b). Compared to approximate CRP's shown in Fig. 5(a), the results from  $J$ -shifting using  $B_{opt}$  in Fig. 5(b) are in much better agreement with exact quantum scattering results.

We calculated the thermal rate constant on the  $^3A''$  surface using both the saddle-point  $B$ -constant and the empirically-adjusted  $B$  constant. Both sets of thermal rate constants are listed in Table 1, and the calculation with the smaller, adjusted  $B$ -constant gives an approximately 30% increase in the thermal rate constant. The rate constant obtained with this  $B$ -constant is used in further comparisons with experiment.

The QM rate constants on both surfaces and their sum are plotted in Fig. 6. At low temperature, the  $^3A'$  surface contributes less than 0.1% to the total rate constant; but its contribution grows gradually with increasing temperature, and contributes to a level of 30% at 3200 K.

The thermal rate constants were also calculated by the ICVT/ $\square$ OMT method over the temperature range 200 - 3200K for both the  $^3A''$  and  $^3A'$  surfaces. The summed rate constant is compared with the summed QM rate constant in Table 2. These approximate rate constants are smaller (by factors of three or more in the temperature range 300-400 K) than the QM results. As the temperature increases the agreement with the QM results improves significantly.

We investigated whether the use of the harmonic approximation in the POLYRATE calculation is responsible for the rather large differences between the QM and ICVT/ $\square$ OMT rate coefficients for the  $^3A''$  surface at low temperature by using the Morse

approximation for the vibrational modes in POYRATE. The resulting rate coefficients are smaller than the ICVT/ $\square$ OMT ones using the harmonic approximation by 2.4% at 200 K and smaller by 1.2% at 600 K. Therefore, the inclusion of anharmonicity in the vibrational modes cannot account for the differences between the low-temperature QM and ICVT/ $\square$ OMT results. Finally, we note that a detailed analysis of the treatment of vibrational modes, reaction paths, and semiclassical treatments of tunneling in the POLYRATE program for the O( $^3$ P) + HCl reaction is presented in Ref. 10, in the context of the KSG and S4 potential surfaces.

The present summed QM and ICVT/ $\square$ OMT rate constants were fit over the temperature range 200 – 3200 K using the standard generalized Arrhenius expression  $BT^a \exp(-c/T)$ , with the results

$$k(T) \text{ (cm}^3 \text{ molecule}^{-1} \text{ s}^{-1}\text{)} = 9.748 \times 10^{-19} T^{2.114} e^{-2025/T} \quad (3)$$

for the QM rate constant and

$$k(T) \text{ (cm}^3 \text{ molecule}^{-1} \text{ s}^{-1}\text{)} = 1.701 \times 10^{-16} T^{1.485} e^{-2957/T} \quad (4)$$

for the ICVT/ $\square$ OMT rate constant. These expressions reproduce the corresponding results tabulated in Table 2 at thirty-one temperatures, with average deviations of 18% and 22%, for the QM and VTST, respectively.

In Fig. 7, the summed QM and ICVT/ $\square$ OMT rate constants are plotted with all the available experimental data.<sup>15,16,23–26</sup> We also present the previous QM rate constant obtained with the S4 potential energy surface. As seen, the present QM results are in very good agreement with experiments from 250 – 2000 K, including the newest ones of Hsiao *et al.*<sup>16</sup> For temperatures above 2000 K there is significant disagreement with the new high-temperature experiments of Hsiao *et al.*<sup>16</sup> A sudden increase in the curvature

of the experimental data points shows up, which cannot be reproduced by either the S4 or the RP surfaces. We discuss possible sources of this disagreement below. The earlier QM calculations on the S4 potential are significantly above experiment (as noted previously<sup>7,8,10</sup>) except at the highest temperatures. Since the QM (S4) calculations do not include the contribution from the  $^3A'$  state, the comparison at temperatures above 1500 K is problematic.

Thus, the present quantum calculations with the new *ab initio* potentials are in very good agreement with experiment over a large temperature range, with the exception of the recent high-temperature experimental results.<sup>16</sup> These new potentials have higher barriers to reaction than any previous potential, including the recent estimates of barrier heights by Hsiao *et al.*<sup>16</sup> The disagreement with the high temperature experimental results are also present in the VTST calculations reported by Hsiao *et al.*, which are quite similar to the present ICVT/ $\square$ OMT ones. However, their calculations were based on local approximations to vibrational modes along the minimum energy paths which, as noted above, predict lower barriers to reaction than the RP potentials.

We have considered several possible explanations for the disagreement between theory and experiment at the highest temperatures noted above. One possibility is the contribution from the channel ClO+H, which is not described in the RP potentials. Another is the possible role of the O( $^1D$ ) + HCl reaction, where O( $^1D$ ) could be formed in inelastic collisions of O( $^3P$ ) with HCl at high collision energies. We now briefly consider both of these possibilities.

As mentioned already, in order to get a converged thermal rate constant at  $T = 3200$  K, the CRP had to be integrated up to a total energy of 2.76 eV, which is well above the

energetic threshold of 1.65 eV for the  $O(^3P) + HCl \rightarrow ClO + H$  reaction channel. As a result, the contribution from this channel to the total rate constant needs to be considered. Unfortunately we do not know the details of the potential for this channel and so we will approximate  $N(E)$  for this reaction channel by the number of open channels for the ClO product, which is given by

$$N(E) = \prod_v \prod_j (2j + 1) \Theta(E_{tot} - E_0 - E_{vj}^{ClO}),$$

where the ro-vibrational energy was evaluated using a separable harmonic oscillator/rigid rotor approximation with  $E_0 = 1.65$  eV. This expression for the CRP is clearly an upper bound, which, however, is very useful in estimating the possible contribution of this channel to the total rate constant. Using this approximation for the CRP for this reaction channel, we obtained a value of  $1.76 \times 10^{-13}$  cm<sup>3</sup>/(molec-sec) at 3200 K, which is roughly 2 orders of magnitude smaller than the total rate constant we obtained ignoring this channel. Thus, we conclude that we are justified in neglecting this channel.

Consider next the  $O(^1D) + HCl \rightarrow \{OH + Cl, ClO + H\}$  reaction. The rate constant of this reaction has been measured<sup>27</sup> and calculated<sup>28</sup> to be of the order of  $1.0 \times 10^{-10}$  cm<sup>3</sup>/(molec-sec) at room temperature and with a very slight dependence on temperature. This value is only slightly larger than the experimentally reported value for the  $O(^3P)$  reaction at 3200 K. The energy difference between  $O(^1D)$  and  $O(^3P)$  is roughly 44 kcal/mol and a simple estimate of the thermal population of  $O(^1D)$  at 3200 K is less than 1% and so the thermal rate from the  $O(^1D)$  reaction, assuming a thermal distribution is roughly  $10^{-13}$  cm<sup>3</sup>/(molec-sec). This is again negligible compared to the

calculated rate constant with  $O(^3P)$ , and so it appears that this reaction can be ruled out as a possible contributor to the high temperature rate constant measurements of Hsiao *et al.*

#### IV. SUMMARY AND CONCLUSIONS

We have reported quantum reactive scattering calculations for the  $O(^3P) + HCl$  reaction on the scaled MRCI+Q/CBS potential energy surfaces obtained by Ramachandran and Peterson<sup>14</sup> for the  $^3A''$  and  $^3A'$  electronic states. Low energy resonances are found in the CRP on the  $^3A''$  surface, but not on the  $^3A'$  surface. Similar structures have been found in the CRP for the S4 surface,<sup>9</sup> and these have been traced to the existence of van der Waals wells in the entrance and exit channels of that potential surface.<sup>13</sup> The RP  $^3A''$  surface also contains van der Waals wells but the  $^3A'$  surface is free of such features. The presence of low energy resonances on the RP  $^3A''$  surface and their absence on the RP  $^3A'$  surface, therefore, lends further support to the conclusion<sup>13</sup> that these low energy resonances are due to the existence of the van der Waals wells on the  $^3A''$  surface.

The QM rate constants are calculated from 200 to 3200 K based on quantum reactive scattering results with a  $J$ -shifting approximation. The accuracy of the  $J$ -shifting approximation on both surfaces is tested, and different improved  $J$ -shifting techniques are applied to achieve better accuracy. The  $^3A'$  surface is shown to have no significant contribution to the total thermal rate constant at lower temperatures, but becomes more and more important with increasing temperature, and reaches a 30% contribution at

3200 K. The comparison of these results with QM rate constants calculated on the S4 surface and with experimental results for  $T < 2000$  K indicates that the reaction barrier on the RP<sup>3</sup>A” surface is closer to the correct value. For temperatures below 2000 K, the present QM results agree very well with the experimental data. The ICVT/□OMT rate constants are not in good agreement with experimental values at lower temperatures, but the agreement between them improves with increasing temperature. However, neither the QM nor the ICVT/□OMT results can account for the sudden change in the curvature of the experimental data points for  $T > 2000$  K. Our analysis in the previous Section rules out the possibility of contributions to the total thermal rate constant from some high energy reaction channels not represented by the two potential surfaces used here. Therefore, we are forced to conclude that the thermal rate constants measured by Hsiao *et al.*<sup>16</sup> for  $T > 2000$  K may contain some errors.

**Acknowledgments:** JMB thanks the Department of Energy (DE-FG02-97ER14782) for financial support. KAP and BR acknowledge the support of the National Science Foundation (CHE-9501262 to KAP and CHE-9712764 to BR).

## References

1. H. Koizumi, G. C. Schatz, and M. S. Gordon, *J. Chem. Phys.* **95**, 6421 (1991).
2. W. H. Thompson and W.H. Miller, *J. Chem. Phys.* **106**, 142 (1996).
3. (a) K. Moribayashi and H. Nakamura, *J. Phys. Chem.*, **99**, 15410 (1995); (b) O. I. Tolstkhin and H. Nakamura, *J. Chem Phys.* **108**, 8899 (1998); (c) O. I. Tolstkhin, K. Nobusada and H. Nakamura, *J. Chem Phys.* **108**, 8922 (1998); (d) K. Nobusada and H. Nakamura, *J. Phys. Chem. A*, **103**, 6715 (1999).
4. B. J. Poirer, *J Chem. Phys.* **108**, 5216 (1998).
5. F. J. Aoiz, L. Bañares, J. F. Castillo, M. Menèdez, and J. E. Verdasco, *Phys. Chem. Chem. Phys.* **1**, 1149. (1999).
6. (a) F. Matzkies and U. Manthe, *J. Chem. Phys.* **110**, 88 (1999); (b) F. Matzkies and U. Manthe, *J. Chem. Phys.* **112**, 130 (2000).
7. S. Skokov, T. Tsuchida, S. Nanbu, J. M. Bowman and S. K. Gray, *J. Chem. Phys.* **113**, 227 (2000).
8. K. Nobusada, H. Nakamura, Y. Lin, and B. Ramachandran, *J. Chem. Phys.* **113**, 1018 (2000).
9. B. Ramachandran, E. A. Schrader III, J. Senekowitsch, and R. E. Wyatt, *J. Chem. Phys.* **111**, 3862 (1999).
10. S. Skokov, S. Zou, J. M. Bowman, T. C. Allison, D. G. Truhlar, Y. Lin, B. Ramachandran, B. C. Garrett, and B. J. Lynch, *J. Phys. Chem. A* **105**, 2298 (2001).
11. Y.-Y. Chuang, J. C. Corchado, P. Fast, L. Villà, W.-P. Hu, Y.-P. Liu, G. C. Lynch, C. F. Jackels, K. A. Nguyen, M. Z. Gu, M. Z.; I. Rossi, E. L. Coitiño, C. Clayton, V. S.

Melissas, B. J. Lynch, R. Steckler, B. C. Garrett, A. D. Isaacson, and D. G. Truhlar, POLYRATE-version 8.4.1, University of Minnesota, MN, 1998.

12. J. M. Bowman, *J. Phys. Chem.* **95**, 4960 (1991).
13. T. Xie, D. Wang, J. M. Bowman, and D. E. Manolopoulos, *J. Chem. Phys.* **116**, 7461 (2002).
14. B. Ramachandran, K. A. Peterson, *J. Chem. Phys.* preceding paper (2003).
15. K. Takahashi, A. Onosaka, K. Saito, and T. Inomata, in *Proceedings of the 23<sup>rd</sup> International Symposium on Shock Waves*, F. K. Lu Ed., Springer-Verlag, Heidelberg, pp. 260-267 (2002).
16. C. C. Hsiao, Y. P. Lee, N. S. Wang, J. H. Wang, and M. C. Lin, *J. Phys. Chem.* **106**, 10231 (2002).
17. D. Skouteris, J. F. Castillo, and D. E. Manolopoulos, *Comput. Phys. Commun.* **133**, 128 (2000).
18. K. A. Nguyen, C. F. Jackels, and D. G. Truhlar, *J. Chem. Phys.* **1996**, 104, 6491.
19. Truhlar, D. G.; Isaacson, A. D.; Garrett, B. C. In *Theory of Chemical Reaction Dynamics*; Baer M., Ed.; CRC Press, Boca Raton, FL, 1985; Vol. 4, pp. 65-137.
20. A.D. Isaacson, M.T. Sund, S.N. Rai, and D.G. Truhlar, *J. Chem. Phys.* **82**, 1338 (1985).
21. Y.-P. Liu, D.-h. Lu, A. González-Lafont, D.G. Truhlar, and B.C. Garrett, *J. Am. Chem. Soc.* **115**, 7806 (1993).
22. D. H. Zhang and J. Z. H. Zhang, *J. Chem. Phys.* **110**, 7622 (1999).
23. R. D. H. Brown and I. W. M. Smith, *Int. J. Chem. Kinet.* **7**, 301 (1975).
24. D. Singleton and R. Cvetanovic, *Int. J. Chem. Kinet.* **13**, 301 (1977).
25. W. Hack, G. Mex, and H. G. Wagner, *Ber. Bunsenges. Phys. Chem.* **81**, 677

(1977).

26. K. Mahmud, J. S. Kim, and A. Fontijn, *J. Phys. Chem.* **94**, 2994 (1990).
27. P. H. Wine, J. R. Wells, and A. R. Ravishankara, *J. Chem. Phys.* **84**, 1349 (1986).
28. M. Bittererová, J. M. Bowman, and K. Peterson, *J. Chem. Phys.* **113**, 6186 (2000).

TABLE 1. The thermal rate constants on the  $^3A''$  surface calculated by using two different B constants (in  $\text{cm}^{-1}$ ) in the *J*-shifting approximation

T (K)	B=0.246	B=0.189	T (K)	B=0.246	B= 0.189
200	2.86E-18	3.72E-18	1800	2.59E-12	3.37E-12
300	1.41E-16	1.83E-16	1900	3.00E-12	3.91E-12
400	1.53E-15	1.99E-15	2000	3.44E-12	4.49E-12
500	7.55E-15	9.84E-15	2100	3.90E-12	5.08E-12
600	2.40E-14	3.12E-14	2200	4.37E-12	5.69E-12
700	5.76E-14	7.51E-14	2300	4.85E-12	6.32E-12
800	1.15E-13	1.50E-13	2400	5.35E-12	6.97E-12
900	2.03E-13	2.64E-13	2500	5.85E-12	7.62E-12
1000	3.25E-13	4.23E-13	2600	6.35E-12	8.27E-12
1100	4.83E-13	6.29E-13	2700	6.85E-12	8.93E-12
1200	6.79E-13	8.85E-13	2800	7.36E-12	9.59E-12
1300	9.13E-13	1.19E-12	2900	7.86E-12	1.02E-11
1400	1.18E-12	1.54E-12	3000	8.35E-12	1.09E-11
1500	1.49E-12	1.94E-12	3100	8.84E-12	1.15E-11
1600	1.83E-12	2.38E-12	3200	9.32E-12	1.21E-11
1700	2.19E-12	2.86E-12			

TABLE 2. QM and ICVT/ $\rho$ OMT rate constants over the temperature range 200-3200 K.

T (K)	QM	ICVT/ $\rho$ OMT	T (K)	QM	ICVT/ $\rho$ OMT
200	3.72E-18	1.68E-19	1800	4.07E-12	3.35E-12
300	1.84E-16	2.88E-17	1900	4.78E-12	3.80E-12
400	2.01E-15	5.79E-16	2000	5.54E-12	4.26E-12
500	1.00E-14	4.10E-15	2100	6.32E-12	4.75E-12
600	3.22E-14	1.64E-14	2200	7.15E-12	5.25E-12
700	7.86E-14	4.65E-14	2300	8.00E-12	5.75E-12
800	1.59E-13	1.06E-13	2400	8.89E-12	6.28E-12
900	2.84E-13	2.04E-13	2500	9.79E-12	6.81E-12
1000	4.62E-13	3.54E-13	2600	1.07E-11	7.36E-12
1100	6.97E-13	5.64E-13	2700	1.16E-11	7.91E-12
1200	9.95E-13	8.38E-13	2800	1.26E-11	8.47E-12
1300	1.36E-12	1.18E-12	2900	1.34E-11	9.05E-12
1400	1.78E-12	1.60E-12	3000	1.44E-11	9.62E-12
1500	2.27E-12	2.10E-12	3100	1.53E-11	1.02E-11
1600	2.81E-12	2.50E-12	3200	1.62E-11	1.08E-11
1700	3.42E-12	2.91E-12			

## Figure captions

**FIG. 1.** The  $J = 0$  CRP on the  ${}^3A''$  and  ${}^3A'$  surfaces plotted against the total energy.

**FIG. 2.** The comparison between  $J = 0$  and  $J=1$  (even parity) CRP on the  ${}^3A''$  surface.

**FIG. 3.** The convergence of the  $J = 50, P = -1$  CRP with respect to different  $K_{max}$  values.

**FIG. 4.** The comparison of the exact  $J = 50, P = -1$  CRP to that calculated by the 'J-shifting' approximation.

**FIG. 5.** The comparison of exact CRPs to the CRP calculated from the  $J$ -shifting approximation with two different  $B$  constants. (a)  $B_{rot} = 3.062 \times 10^{-5}$  eV, (b)  $B_{rot} = 2.35 \times 10^{-5}$  eV.

**FIG. 6.** The QM thermal rate constants on the  ${}^3A'$  and  ${}^3A''$  surfaces, and the total thermal rate constant.

**FIG. 7.** The comparison of the QM and ICVT/ $\square$ OMT thermal rate constants on the RP surface with all the available experimental data and the QM thermal rate constant on the S4 surface over the temperature range 250–3200K. (For experimental data:  $\_$  Ref. 15,  $\square$  Ref. 16,  $\_$  Ref. 23, \* Ref. 24,  $\_$  Ref. 25,  $\_$  Ref. 26,)

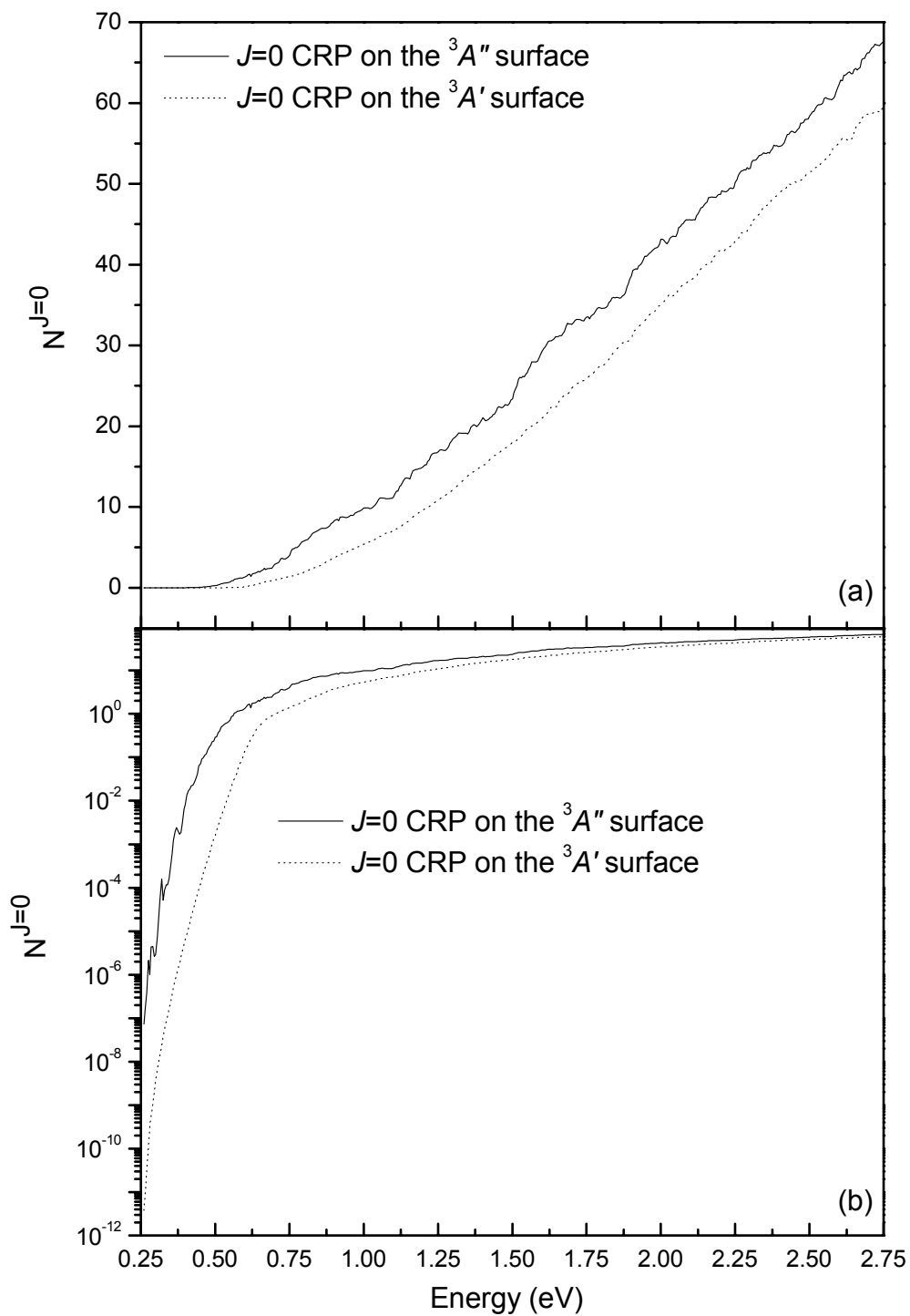


FIG 1.

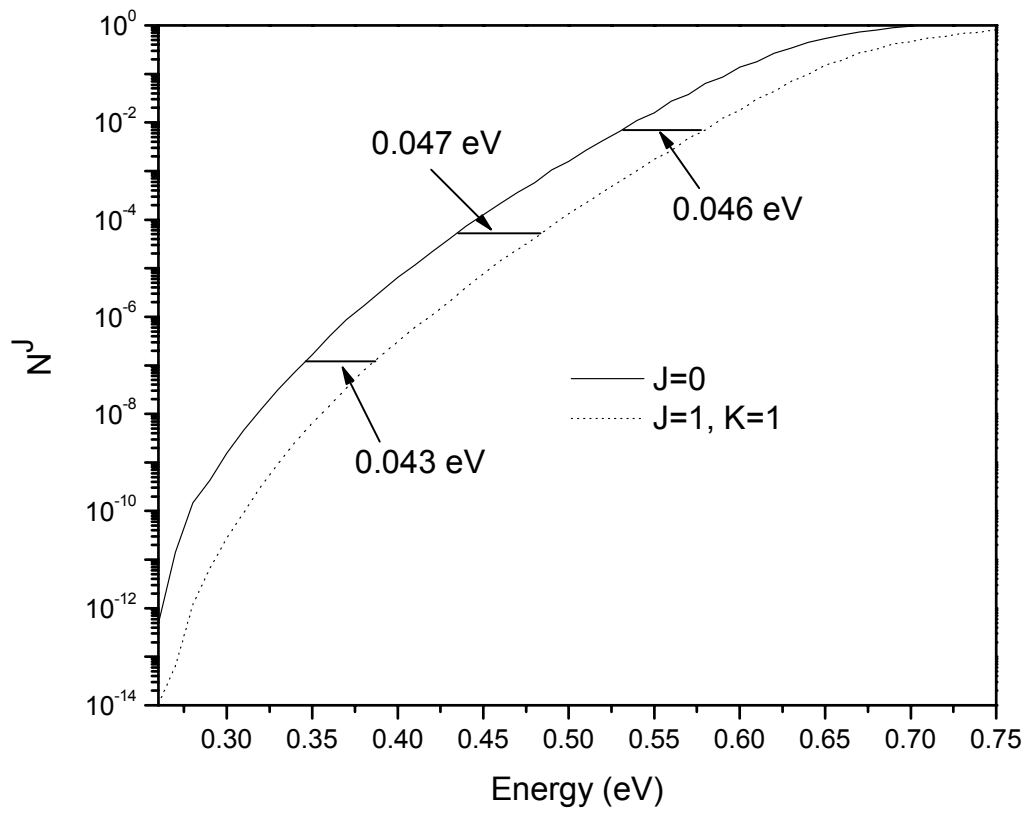


FIG 2.

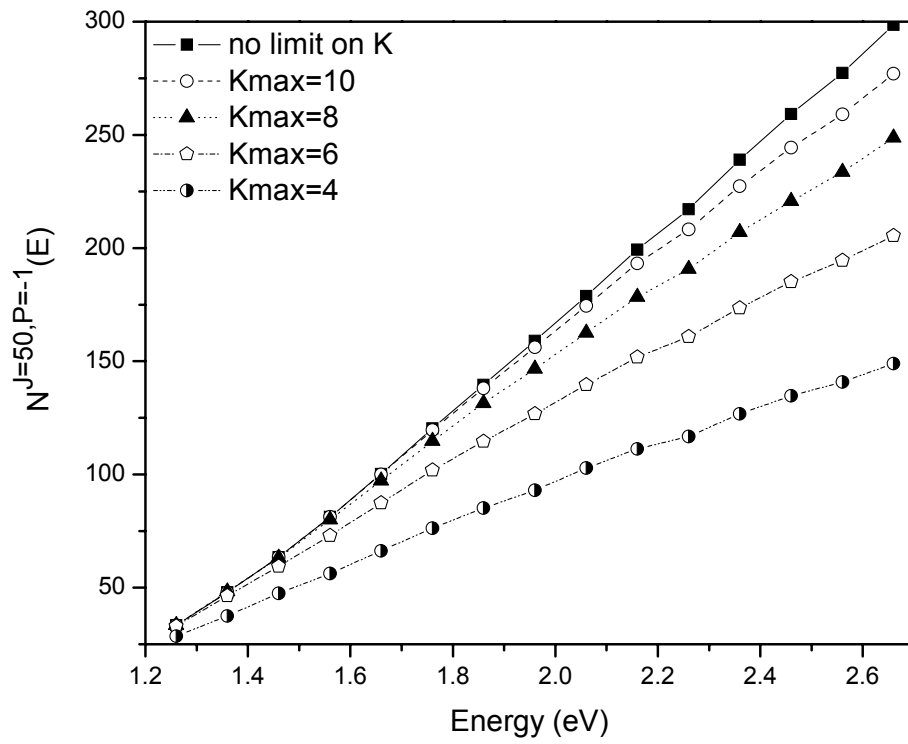
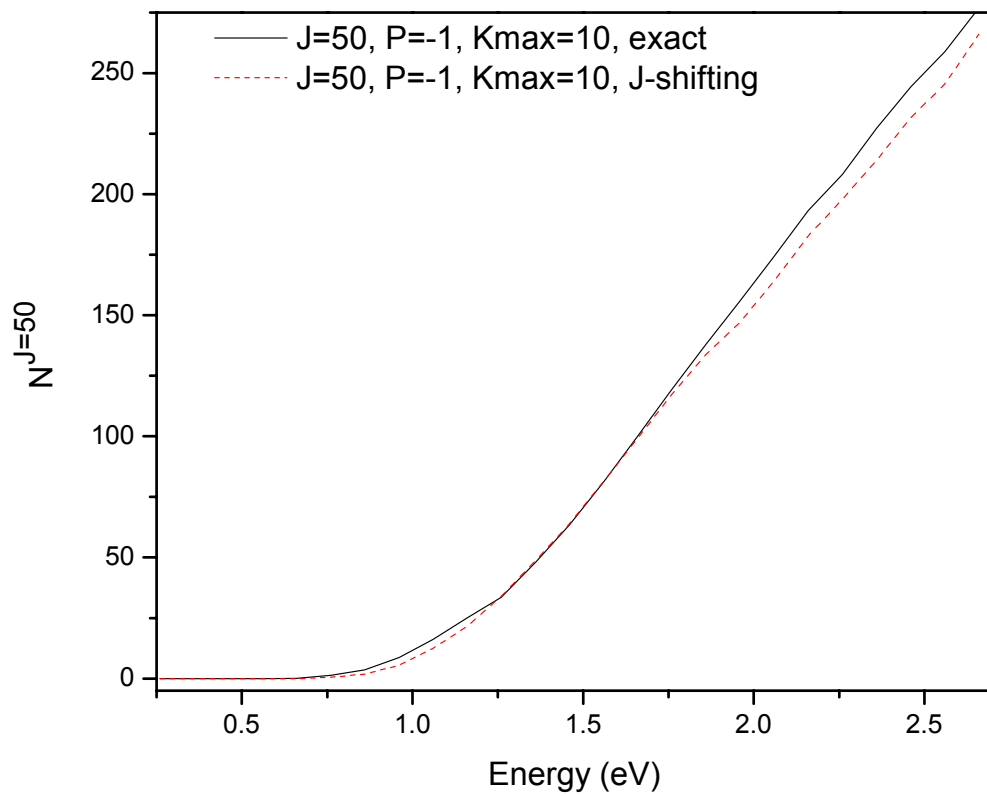


Fig 3.



**Fig 4.**

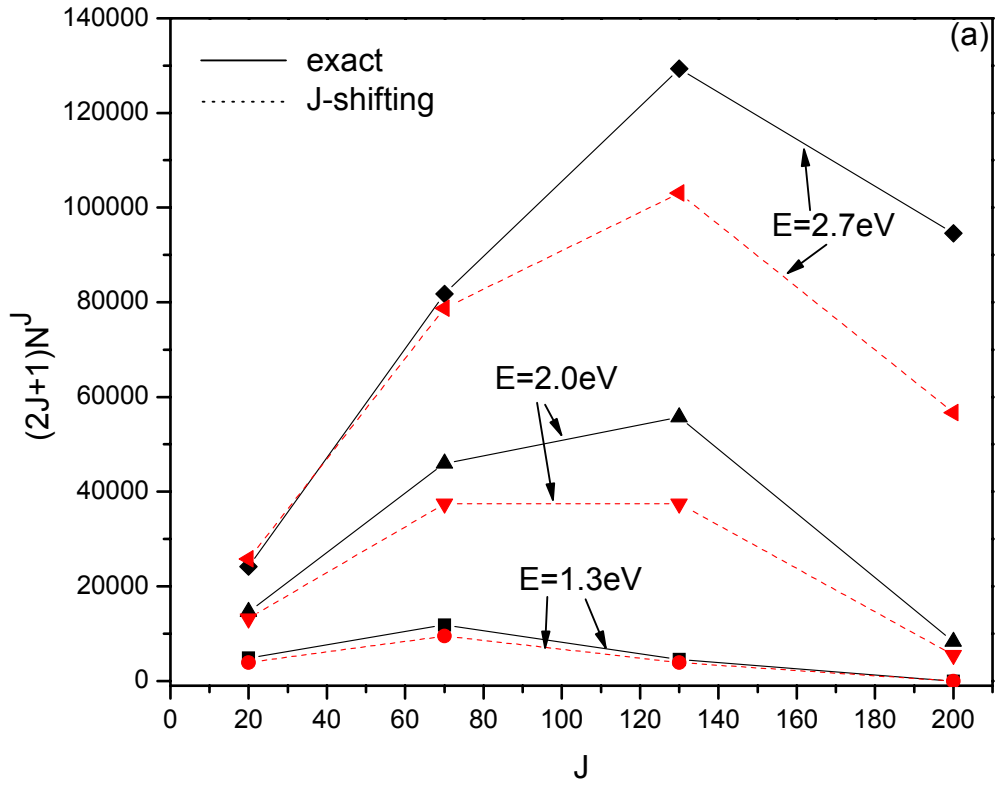


Fig 5(a).

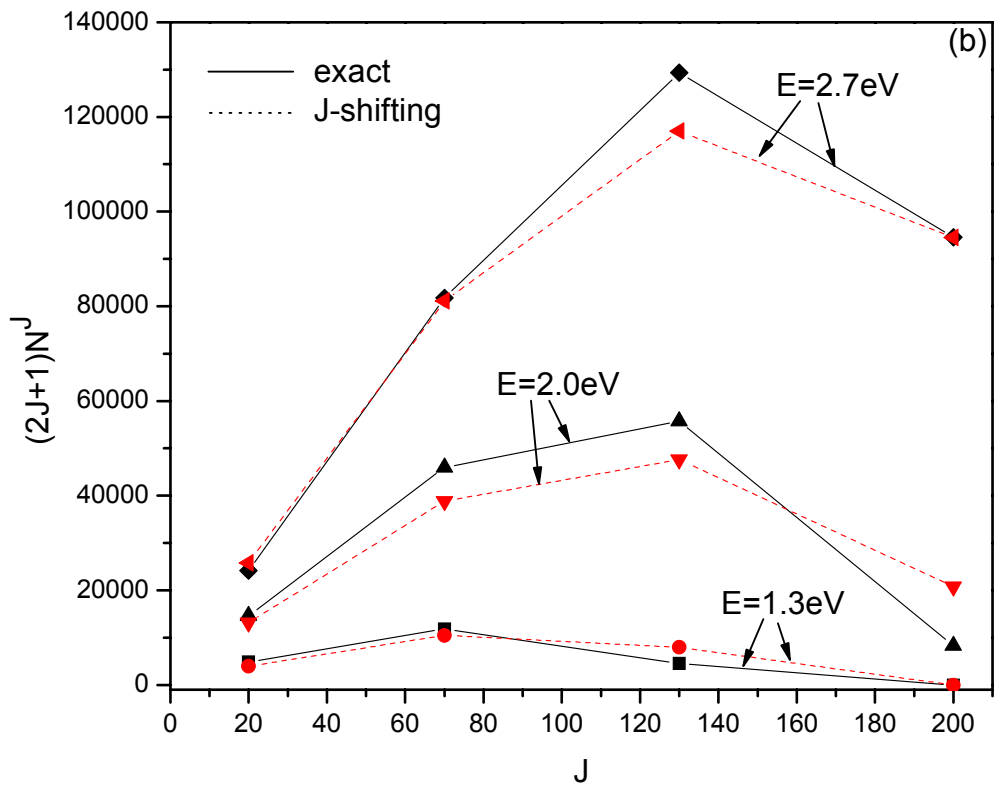


Fig 5(b).

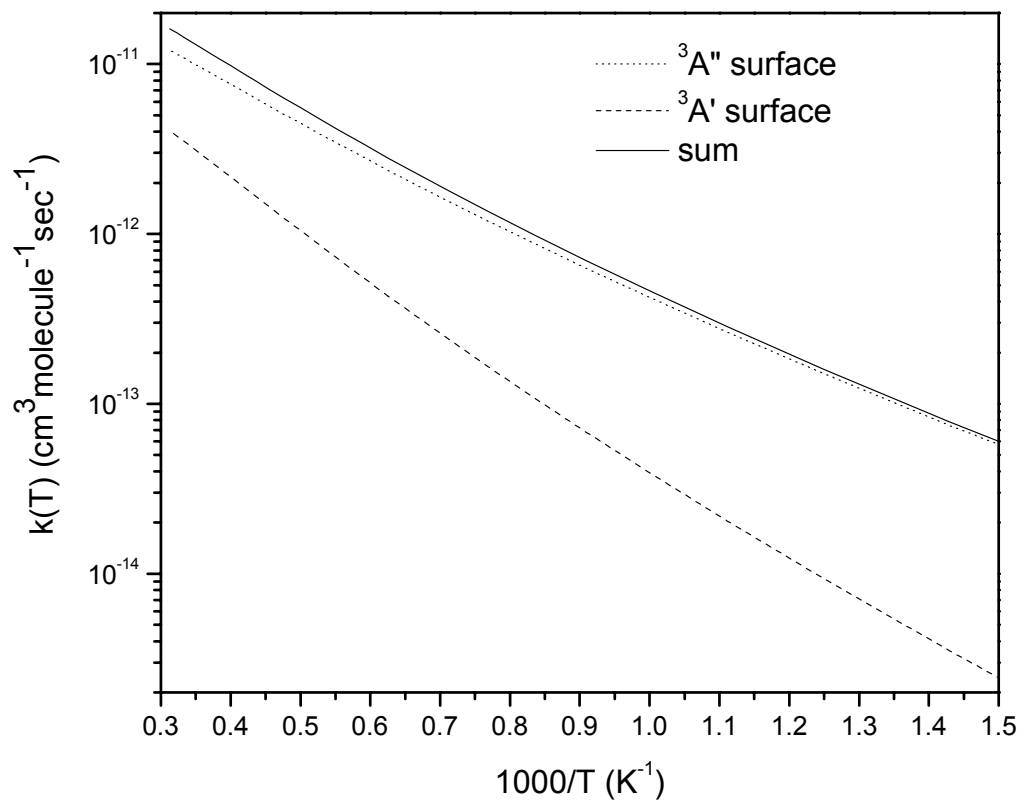


Fig 6.

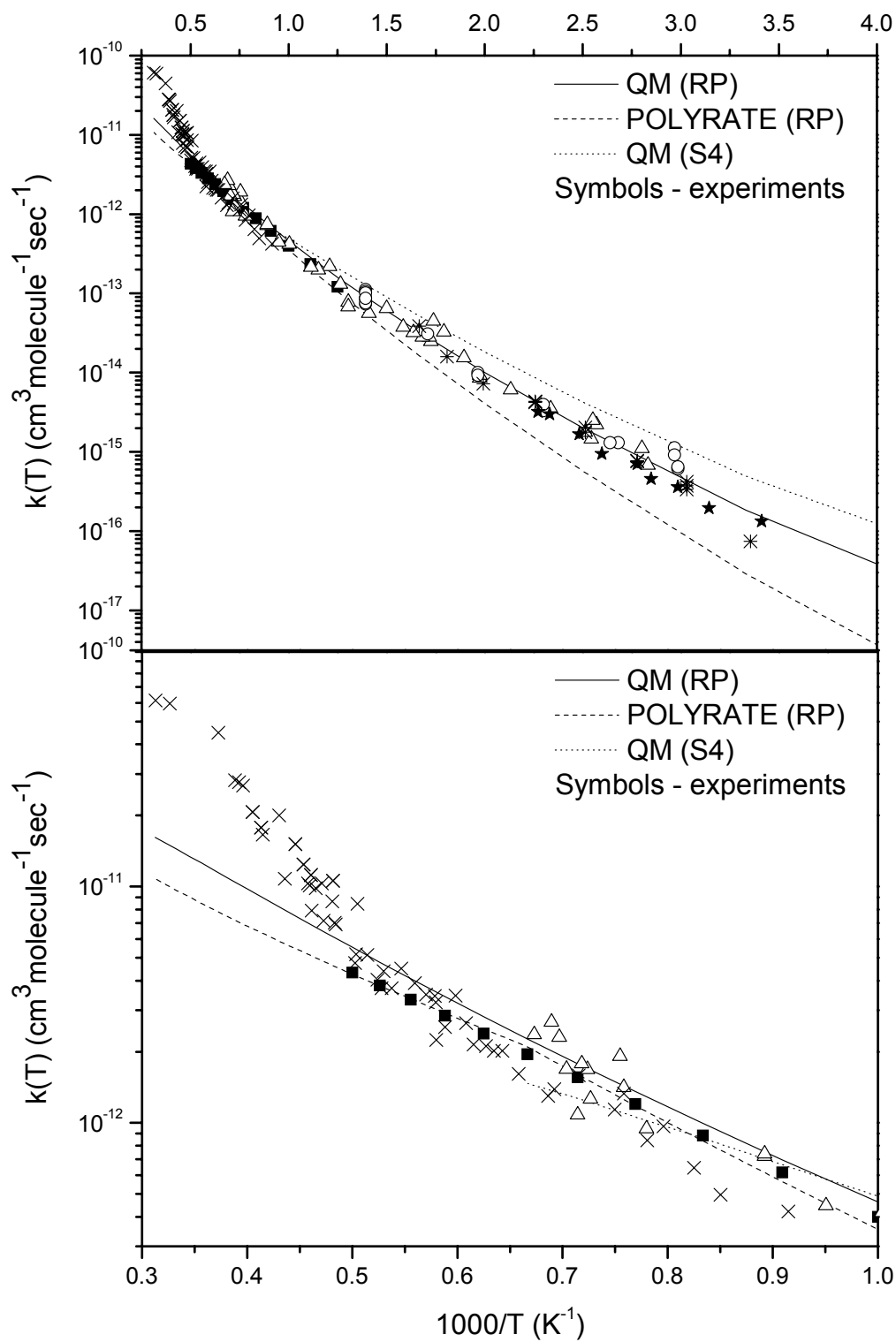


FIG 7.